

Cite this: *J. Mater. Chem. A*, 2019, 7, 1069

# Constructing stable ordered ion channels for a solid electrolyte membrane with high ionic conductivity by combining the advantages of liquid crystal and ionic liquid†

Shi Wang,‡ Qinghui Zeng,‡ Ailian Wang, Xu Liu, Jie Chen, Zhinan Wang and Liaoyun Zhang \*

The advantages of solid-state polymer electrolytes (SPEs) such as ease of fabrication, high safety, good compatibility with Li metals make SPEs one of the most promising electrolyte materials for next generation high-performance and high-safety lithium-ion batteries (LIBs). However, the traditionally used PEO-based electrolytes usually exhibit very low ionic conductivity due to the high crystallinity of PEO, which impedes the commercialization of solid-state LIBs using PEO-based polymer electrolytes. In this study, an 'alternative' solid electrolyte material was prepared using a nematic liquid crystal (LC) and an ionic liquid (IL). Specifically, the LC with ordered layered nanostructures was polymerized and immobilized via UV-irradiation, while IL was sufficiently inserted into the ordered ion channels for fast transport ions. It should be noted that such a free-standing electrolyte film with stable ordered channels has been confirmed through the characterizations of DSC, POM, SEM and XRD. As a result, the solid electrolyte film shows superior comprehensive electrochemical performance in terms of a very high room temperature ionic conductivity ( $2.14 \times 10^{-2} \text{ S cm}^{-1}$ ), wide electrochemical window (4.8 V), and very good compatibility with lithium metal. Furthermore, the  $\text{LiFePO}_4/\text{Li}$  cell using the ordered electrolyte film shows an average discharge capacity of  $150 \text{ mA h g}^{-1}$ . Undoubtedly, our study provides a new solid electrolyte material that has the potential to be used in the next generation of high safety and high energy density LIBs.

Received 1st October 2018  
Accepted 5th December 2018

DOI: 10.1039/c8ta09489f

rsc.li/materials-a

## Introduction

The advantages such as design flexibility, high operating potential, high energy density and long service life make rechargeable lithium-ion batteries (LIBs) one of the most crucial electrical energy storage devices.<sup>1,2</sup> However, numerous problems still need to be overcome to obtain LIBs with enhanced electrochemical performance and improved safety. In particular, the extensively used organic liquid electrolytes show extremely high volatility, potential leakage and high flammability, which results in shortened service life and safety risk (even explosion hazard) of LIBs (particularly used under high temperatures and on a large scale).<sup>3,4</sup> Solid polymer electrolytes (SPEs) can be an effective solution for the above problems, particularly the safety issues.<sup>5-7</sup>

Among all the SPEs, the typically and widely studied polymer electrolyte matrices are poly(ethylene oxide) (PEO) and its derivatives due to the advantages such as ease of fabrication, high safety, and good compatibility with Li salts.<sup>8</sup> However, the high crystallinity of PEO contributes to the very low room temperature ionic conductivity of the corresponding polymer electrolyte,<sup>9,10</sup> which impedes the commercialization of solid-state LIBs using PEO-based polymer electrolytes. Therefore, developing and studying new 'alternate' electrolyte materials with superior comprehensive electrolyte performance are still very necessary.

To date, alternative SPE matrices of PEO such as polycarbonates, polyesters, polynitriles, polyalcohols, and polyamines have been widely studied and shown some satisfactory results.<sup>11</sup>

Liquid crystals (LCs) combine the flowing properties of isotropic liquids and order of crystalline solids, resulting in a very unique material.<sup>12</sup> The molecules can self-assemble into a range of liquid crystal nanostructures (spontaneous induction of phase segregation) by adjusting the molecular shape and intermolecular interactions.<sup>13-15</sup> This indicates that LC materials are promising nominees for fast transport of ions.<sup>16</sup> More importantly, it is found that the LC materials with ordered

School of Chemical Sciences, University of Chinese Academy of Sciences, Beijing 100049, China. E-mail: zhangly@ucas.ac.cn

† Electronic supplementary information (ESI) available: POM images of LC, ionic conductivities of PLC-IL-1-1, PLC-IL-1-2 and PPEGDA/LiTFSI, striping/plating curves of Li/PLC-IL-1-2/Li cell, coulombic efficiency of the LFP/PLC-IL-1-1/Li and LFP/PLC-IL-1-2/Li cells, rate property of LFP/PLC-IL-1-2/Li cell. See DOI: 10.1039/c8ta09489f

‡ Shi Wang and Qinghui Zeng contributed equally to this work.

structures can be used as safe and efficient electrolytes.<sup>17</sup> LCs have served as template inorganic and organic materials, which significantly increase the carrier mobility.<sup>18,19</sup> It is widely known that the PEO-based polymer electrolytes usually have ionic conductivities lower than  $10^{-5}$  S cm<sup>-1</sup> at room temperature.<sup>8,20</sup> Interestingly, through constructing faster ion channels using LC, the as-prepared LC-based polymer electrolyte film exhibits a high ionic conductivity of  $10^{-3}$  S cm<sup>-1</sup> at room temperature (the value is very close to the ionic conductivity of liquid electrolytes),<sup>21</sup> indicating the crucial role of ion channels in improving the ionic transport efficiency. Moreover, Kato *et al.* focused on the liquid crystal-based electrolytes due to the inherent orientation ability of liquid crystal materials, which can be used to construct ordered ion pathways for more efficient transport of ions.<sup>16,21–25</sup> Very recently, we also designed and synthesized a series of liquid crystal-based polymer electrolyte materials with ordered ion channels for efficient transport of ions, which generally showed satisfactory cell performance when used in LIBs.<sup>26–29</sup>

Based on the above mentioned advantages of LC-based materials used as electrolytes and our recent studies, we tried to further design and synthesize a novel liquid crystal monomer, which should have high orientation ability for constructing ordered structures. More importantly, such ordered structures need to be effectively immobilized, *i.e.*, the special LC monomer should polymerize under certain conditions. In this regard, the 1,4-bis(4-(6'-acryloxy-hexyloxy)benzoyloxy)-2-toluene (C6M) was selected and synthesized, which not only shows nematic phase but also has the active terminal double bond that can be sufficiently polymerized under ultra violet (UV) irradiation.<sup>30</sup> As a result, a polymeric LC with ordered layered nanostructures can be obtained and immobilized.

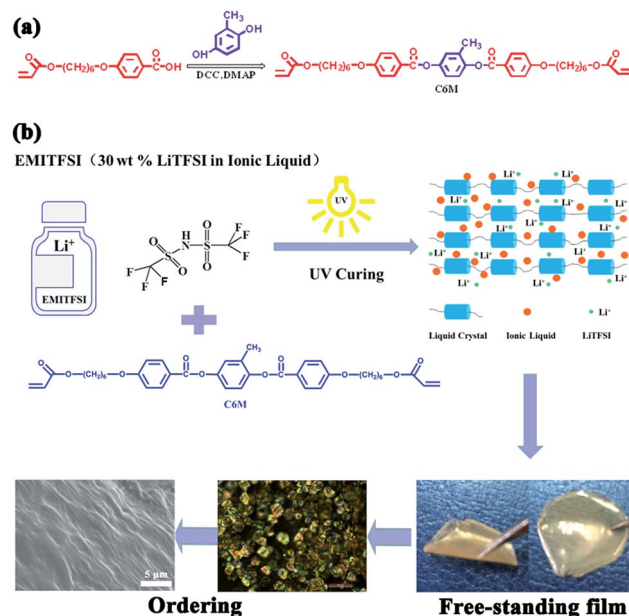
Nevertheless, such an ordered structure is not enough to reach the goal of effective transport of ions. Therefore, an effective ion transport medium is necessary. Of particular interest, ionic liquids (ILs) with the unique properties of low flammability, ultralow volatility, good thermal stability and ionic conductivity have drawn our attention.<sup>31</sup> Furthermore, it has also been demonstrated that ILs can be a promising electrolyte matrixes for LIBs.<sup>32–35</sup>

Thus, in this study, a novel solid electrolyte with highly ordered ion channels was prepared using a nematic liquid crystal (C6M), an ionic liquid (1-ethyl-3-methylimidazolium bis(trifluoromethylsulfonyl)imide) and a lithium salt. Specifically, the free-standing solid-state composite polymer electrolyte film with highly ordered layered nanostructures was obtained through photopolymerization of the LC monomer. Furthermore, IL was inserted into the layered nanostructures to transport ions. It should be noted that the LC was not only used as the active monomer to polymerize, but also acted as a highly ordered template (the orientation feature of LC can construct ordered structure) to provide ion channels. As a result, the solid-state electrolyte film with ion channels shows superior comprehensive electrochemical properties. More importantly, we also confirmed that the novel and free-standing solid electrolyte film can be used in LIBs. Specifically, the LiFePO<sub>4</sub> (LFP)/Li cell using the ordered electrolyte film shows superior cell

performance. To the best of our knowledge, such a special solid electrolyte with excellent cell performance has not been reported. Our results provide a novel solid electrolyte material with highly ordered ion channels using liquid crystal and ionic liquid, which can be promisingly applied in solid LIBs.

## Results and discussion

The LC monomer was synthesized *via* the esterification reaction of 4-(6'-acryloxy-hexyloxy) benzoic acid and 2-methyl-hydroxy phenol while using *N,N*-dicyclohexyl carbodiimide (DCC) as a dehydrant and 4-dimethylaminopyridine (DMAP) as a catalyst (see the synthesis route in Scheme 1a). In addition, Fig. 1a provides the nuclear magnetic resonance hydrogen spectrum (<sup>1</sup>H NMR) of the as-prepared LC monomer. The characteristic peaks belonging to unsaturated hydrocarbon bonds (–CH=CH<sub>2</sub>) appear at the chemical shift of 6.38 (peak f), 6.15–6.08 (peak g), and 5.84–5.81 (peak h) ppm. The saturated hydrocarbon bonds are denoted by chemical shifts at 4.17 (peak i), 4.04 (peak j), 2.23 (peak k), 1.84 (peak l), 1.72 (peak m) and 1.66–1.36 (peak n) ppm. In addition, the peaks at 8.11 (peak a), 7.17–7.05 (peak c, d, and e), and 6.96 (peak b) ppm are ascribed to aromatic hydrogens. The <sup>1</sup>H NMR spectrum of LC indicates that LC has been successfully synthesized. The structural information of the LC was further elucidated by Fourier transform infrared (FTIR) spectroscopy. As can be seen in Fig. 1b, the saturated hydrocarbon stretching vibration of –CH<sub>2</sub>– and –CH<sub>3</sub> appears at 2937, 2865 cm<sup>-1</sup>,<sup>36</sup> respectively. The skeletal vibration of the benzene ring shows characteristic peaks at 1600 and 1500 cm<sup>-1</sup>.<sup>37</sup> Additionally, the IR absorption peaks at 3071 and 1633 cm<sup>-1</sup> come from the CH<sub>2</sub>=CH–.<sup>36,38,39</sup> Combining the <sup>1</sup>H NMR and FTIR characterizations, we conclude that the LC



**Scheme 1** (a) Synthesis route of the liquid crystal (LC, C6M) monomer. (b) Preparation of the free-standing composite solid-state electrolyte film using LC and IL with ordered ion channels.

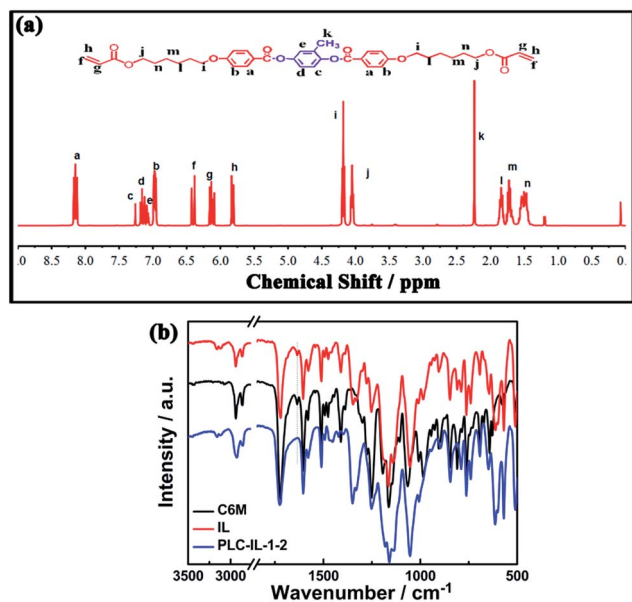


Fig. 1 (a)  $^1\text{H}$  NMR of LC. (b) IR spectra of LC, IL and the prepared solid electrolyte film.

monomer has been obtained *via* an esterification reaction of 4-(6'-acryloxy-hexyloxy) benzoic acid and 2-methyl-hydroxy phenol. Subsequently, a free-standing solid-state composite polymer electrolyte film with highly ordered layered nanostructures was obtained through photopolymerization of the LC monomer with IL inserted into the layered nanostructures to transport ions (Scheme 1b). It should be noted that LC was not only used as the active polymerable monomer but also acted as a highly ordered template to provide ion channels. The free-standing electrolyte film (PLC-IL-1-2, '1-2' represents the weight ratio of LC and IL is 1/2) was characterized by FTIR spectroscopy (Fig. 1b). It was found that the characteristic absorption peaks of  $\text{CH}_2=\text{CH}-$  at  $3071$  and  $1633\text{ cm}^{-1}$  completely disappear, confirming the sufficient polymerization of the activated carbon-carbon double bond in the LC monomer under UV radiation. Furthermore, as predicted, the absorption peaks belonging to the benzene ring and saturated hydrocarbon are retained. It should be noted that the shoulder peaks at  $3166$  and  $3122\text{ cm}^{-1}$  are ascribed to the imidazole ring of the IL.<sup>40</sup> Thus, the shoulder peaks appear on the IR spectrum of PLC-IL-1-2.

The liquid crystal feature of LC can be generally analyzed by differential scanning calorimeter (DSC) and polarizing optical microscopy (POM). Fig. 2a shows the DSC curves of the LC monomer in the temperature range from  $-90$  to  $150\text{ }^\circ\text{C}$ . During the heating process, two exothermic peaks appear at  $11$  and  $34\text{ }^\circ\text{C}$  due to the cold crystallization.<sup>41</sup> A high intensity endothermic peak is seen at  $60\text{ }^\circ\text{C}$  and a low intensity endothermic peak is also observed at  $81\text{ }^\circ\text{C}$  on the DSC curve, which can be attributed to a typical mesophase (from  $60$  to  $80\text{ }^\circ\text{C}$ ). According to the DSC heating curve, another phase transformation is observed from  $81$  to  $117\text{ }^\circ\text{C}$ . During the cooling process, the nematic phase is seen in a wider temperature range (from  $9$  to

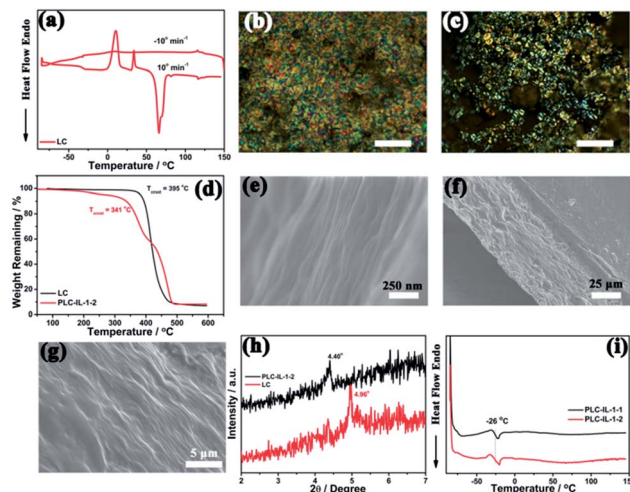


Fig. 2 (a) DSC curves of the LC from  $-90$  to  $150\text{ }^\circ\text{C}$ . (b) POM image of LC at the original  $30\text{ }^\circ\text{C}$ . (c) POM image of PLC-IL-1-2. (d) TGA curves of LC and PLC-IL-1-2. (e) SEM image of the solid electrolyte film (PLC-IL-1-2, on the surface), which shows very ordered layered nanostructures. (f) and (g) show the cross section of the solid electrolyte film at different magnifications, which also exhibits obvious layered nanostructures. (h) XRD profiles of LC and PLC-IL-1-2. (i) DSC curves of the solid-state electrolyte films (PLC-IL-1-1 and PLC-IL-1-2).

$116\text{ }^\circ\text{C}$ ).<sup>42</sup> The phase transformation process of the LC monomer can be directly observed using POM. Fig. S1† shows the POM images of the LC during heating and cooling processes. The typical nematic phase is seen from room temperature (also shown in Fig. 2b) to  $65\text{ }^\circ\text{C}$  on heating and also observed from room temperature to  $0\text{ }^\circ\text{C}$  on cooling. Generally, the DSC and POM characterizations indicate that the LC molecules tend to uniaxially align along the common director, which can be directly used to construct ordered ion channels in polymer electrolytes.

The POM image of the electrolyte film (PLC-IL-1-2) at room temperature is shown in Fig. 2c. It is clearly seen that the electrolyte film inherits the nematic phase of the LC monomer after UV polymerization. We further evaluated the thermal stability of the series samples (including LC monomer, the as-prepared electrolyte film). The thermal decomposition temperature ( $T_{\text{onset}}$ ) of the LC monomer reaches  $395\text{ }^\circ\text{C}$ , while the electrolyte film has a  $T_{\text{onset}}$  of  $341\text{ }^\circ\text{C}$ . The relatively decreased thermal stability of the electrolyte film can be explained by the relatively low thermal stability of the IL. Nevertheless, the thermal stability of the electrolyte film is still very high, which can meet the application of the electrolyte film in a wide temperature range.

In addition, the highly ordered structure of the electrolyte film can be further observed by scanning electron microscopy (SEM). The electrolyte film (PLC-IL-1-2) exhibits highly ordered layered nanostructures on the surface (Fig. 2e). Amazingly, the ordered nanostructures are also formed on the cross section of the film (Fig. 2f). Such highly ordered layered nanostructures can be seen more clearly at higher magnification (compared with Fig. 2f) on the cross section (Fig. 2g). Moreover, as

predicted, a clear X-ray diffraction peak appears at  $2\theta = 4.40^\circ$  (corresponding to the 2 nm  $d$ -spacing between the nanolayers<sup>43</sup>) of the electrolyte film (Fig. 2h), further confirming the successful construction of highly ordered layered nanostructures. The peak of the LC monomer (also shown in Fig. 2h) appears at  $2\theta = 4.96^\circ$  ( $d$ -spacing of 1.8 nm), which indicates that the  $d$ -spacing of the electrolyte film is slightly wider than that of the LC monomer. This is likely because the IL has been sufficiently inserted into the layered nanostructures, causing the increased  $d$ -spacing of the electrolyte film.

According to the DSC, POM, SEM and XRD characterizations, we can confidently conclude that an ordered and layered solid electrolyte membrane has been successfully prepared *via* UV photopolymerization using LC as the active monomer and IL as the transmission medium. Two crucial reasons drive the formation of the solid electrolyte film with ordered ion channels. First, the liquid crystal monomer we synthesized shows a high orientation ability (corresponding to nematic phase). Second, the terminal active double bonds can polymerize under the UV-irradiation, which can make the LC monomer form a free-standing film as well as immobilize the ordered liquid crystal structure. The vivid ionic transport model of the ordered electrolyte film can be seen in Scheme 1b.

If the ordered layered structures were immobilized, it should have had no phase transition corresponding to the mesophase of LC on the DSC curves of the electrolyte films. The DSC curves of PLC-IL-1-1 ('1-1' represents the weight ratio of LC and IL is 1/1) and PLC-IL-1-2 are shown in Fig. 2i. No peaks are observed on the curves except the peaks belonging to the glass transition temperature at  $\sim -26^\circ\text{C}$ , suggesting the effective immobilization of the ordered layered structures of the electrolyte films.

We compared the ionic conductivities of PLC-IL-1-1 with PLC-IL-1-2 (we did not further increase the content of IL due to the poor film forming ability of higher content of IL) at a given temperature (from 25 to 80 °C), which was also fitted by the VTF model (see the equation in the Experimental section). According to the fitting results, the activation energy ( $E_a$ ) values of PLC-IL-1-1 and PLC-IL-1-2 are 5.54 and 1.30 kJ mol<sup>-1</sup>, respectively. It is seen that the  $E_a$  value of PLC-IL-1-1 is over 4 times higher than that of PLC-IL-1-2. A lower  $E_a$  value is more beneficial to the efficient transport of ions. Therefore, PLC-IL-1-2 generally exhibits higher ionic conductivity at a given temperature (from 25 to 30 °C) than that of PLC-IL-1-1. Clearly, the ionic conductivity of PLC-IL-1-2 is  $2.14 \times 10^{-2} \text{ S cm}^{-1}$  at 25 °C, which is much higher than that of PLC-1-1 ( $3.57 \times 10^{-3} \text{ S cm}^{-1}$ , 25 °C). However, the ionic conductivities almost reach the same value at 80 °C, which can be attributed to the negligible ion transport energy barrier at much higher temperatures. It is also known that higher  $E_a$  values usually results in physical characteristics (such as ionic conductivity) of samples showing more sensitivity to temperature. Thus, the ionic conductivity of PLC-IL-1-2 seems to improve slowly with the rise in temperature. For comparison, we also measured the ionic conductivity of the poly(ethylene glycol)diacrylate (PPEGDA)/30% LiTFSI electrolyte film. As can be seen in Fig. S2,† the liquid crystal-based electrolyte film shows much higher ionic conductivity than that of the PPEGDA-based electrolyte film at a given temperature from

30 to 80 °C (for instance, the ionic conductivity of the PPEGDA-based film is  $7.93 \times 10^{-6} \text{ S cm}^{-1}$  at 30 °C), indicating the crucial role of the ordered structure in improving the ionic conductivity of the liquid crystal-based electrolyte film. In addition, the electrochemical window of PLC-IL-1-1 (Fig. 3b, 4.7 V) and PLC-IL-1-2 (Fig. 3c, 4.8 V) is very close, indicating the good electrochemical stability of the electrolyte films using LC and IL.

It is still very necessary to assess the interface compatibility between electrolyte film and lithium metal. Herein, PLC-IL-1-2 was selected to be studied. As shown in Fig. 3d, the initial areal specific resistance between the Li electrode and the electrolyte film is 1600  $\Omega \text{ cm}^2$ . Then, the values fluctuate from 1300 to 1180  $\Omega \text{ cm}^2$ . At last, it reaches a stable value of  $\sim 1240 \Omega \text{ cm}^2$  in 8 days, demonstrating the good interface compatibility between electrolyte film and lithium metal electrode. We further performed the lithium stripping/plating experiments using a Li/PLC-IL-1-2/Li symmetrical cell (over 500 h, the stripping/plating curves are shown in Fig. S3†). It is seen that the overpotential is only about 0.28 V for the stripping/plating of Li metal in the Li/PLC-based electrolyte/Li cell at the current density of 25  $\mu\text{A cm}^{-2}$  (the overpotential is 0.4 V at 50  $\mu\text{A cm}^{-2}$ ), indicating the relatively stable cycling reversibility and stability for Li stripping/plating in the symmetric cell.

The good cell performance is very crucial for the novel solid electrolyte film with controlled ion channels to be practically used. We assembled the LiFePO<sub>4</sub> (LFP)/Li cell using the PLC-IL-1-2 solid electrolyte film to further confirm that the electrolyte film can be used in lithium-ion batteries (LIBs). Furthermore, LFP/PLC-IL-1-1/Li cell was assembled as a comparison due to the relatively low ionic conductivity. Fig. 4a presents the charge-discharge curves of the two cells at different cycles at 0.2C. Clearly, the cell using PLC-IL-1-2 shows much lower overpotential than that of the cell using PLC-IL-1-1. From the long cycle performance of the two cells, as shown in Fig. 4b, it is also seen that the LFP/PLC-IL-1-2/Li (average discharge capacity of

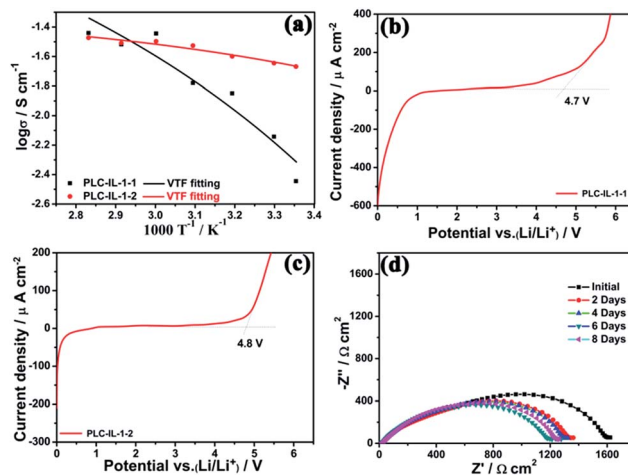


Fig. 3 (a) Ionic conductivities of PLC-IL-1-1 and PLC-IL-1-2 at a given temperature (from 30 to 80 °C). (b) and (c) show the LSV curves of SS/PLC-IL-1-1/SS and SS/PLC-IL-1-2/SS cells, respectively. (d) Electrochemical resistance spectra of Li/PLC-IL-1-2/Li cell after different storage times.

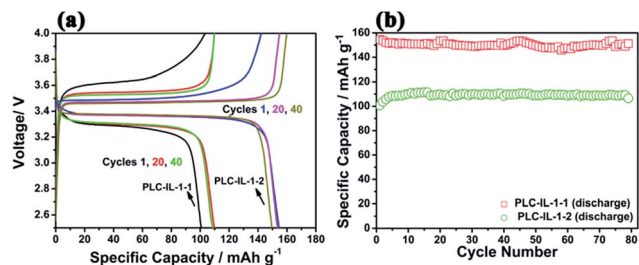


Fig. 4 (a) Charge–discharge curves of the LFP/PLC-IL-1-1/Li and LFP/PLC-IL-1-2/Li cells at the cycle of 1, 20 and 40, respectively. (b) The corresponding cycle performance of the LFP/PLC-IL-1-1/Li and LFP/PLC-IL-1-2/Li cells.

150 mA h g<sup>-1</sup>) cell shows much higher discharge capacity than that of the cell using PLC-IL-1-1 (average discharge capacity of 109 mA h g<sup>-1</sup>). The much better cell performance using PLC-IL-1-2 can be attributed to the higher ionic conductivity and relatively better electrochemical stability of PLC-IL-1-2. Furthermore, both the cells show an average coulombic efficiency of over 95% (Fig. S4†), indicating the very good ability to extract and insert lithium ions of the cell using the liquid crystal-based solid electrolyte with ordered ion channels.

In addition, we further assessed the rate property of the LFP/PLC-IL-1-2/Li cell. As shown in Fig. S5a,† the overpotential at 0.2C is about 0.07 V for the LFP/PLC-IL-1-2/Li cell. Although the overpotential at 0.5 and 1C reaches ~0.14 and ~0.23 V, respectively, due to the polarization effect, it is still very low. The cycle performance of the cell at different current densities can be seen in Fig. S5b,† the discharge capacity reaches 152 mA h g<sup>-1</sup> at 0.2C and the average discharge capacity at 0.5C is 145 mA h g<sup>-1</sup> from cycle 7 to 11. Even at 1C, the discharge capacity is maintained at 130 mA h g<sup>-1</sup>. The average discharge capacity is 141 mA h g<sup>-1</sup> (from cycle 22 to 108) when the current density returns from 1 to 0.5C, indicating the good cyclic reversibility and rate property of the cell using the liquid crystal-based polymer electrolyte (PIL-IL-1-2).

## Conclusion

A novel solid electrolyte with highly ordered ion channels was prepared using a nematic liquid crystal (C6M), ionic liquid (1-ethyl-3-methylimidazolium bis(trifluoromethylsulfonyl)imide) and lithium salt. Specifically, the free-standing solid-state composite polymer electrolyte film with highly ordered layered nanostructures was obtained through photopolymerization of the LC monomer with IL inserted into the layered nanostructures (transport ions). It should be noted that the LC was not only used as the active polymerable monomer but also acted as a highly ordered template to provide ion channels. As a result, the solid-state electrolyte film with ion channels showed a very high room temperature ionic conductivity ( $2.14 \times 10^{-2}$  S cm<sup>-1</sup>), wide electrochemical window (4.8 V), and very good compatibility with lithium metal. More importantly, we also confirmed that the novel and free-standing solid electrolyte film could be used in LIBs. Specifically, the LFP/

Li cell using the ordered electrolyte film showed superior cell performance (average discharge capacity reaches 150 mA h g<sup>-1</sup>). Our results provide a novel solid electrolyte material with highly ordered ion channels using liquid crystal and ionic liquid, which can be promisingly applied in solid LIBs.

## Experimental

### Materials

4-(6'-Acryloxy-hexyloxy) benzoic acid (95%, Meryer), 1-ethyl-3-methylimidazolium bis(trifluoromethylsulfonyl)imide (ionic liquid (IL), 97%, Aladdin), 2-methyl-hydroxy phenol (98%, Aladdin), *N,N*-dicyclohexyl carbodiimide (DCC, 99%, Aladdin), 4-dimethylaminopyridine (DMAP, 99%, Aladdin), hydrochloric acid (HCl, Beijing Chemical Works), sodium bicarbonate (NaHCO<sub>3</sub>, AR, Macklin), PEGDA ( $M_n = 1000$  g mol<sup>-1</sup>, Aladdin) and isopropanol (AR, Macklin) were used as received. Dichloromethane (CH<sub>2</sub>Cl<sub>2</sub>, AR, Beijing Chemical Works) and tetrahydrofuran (THF, AR, Beijing Chemical Works) were dried with CaH<sub>2</sub> and distilled prior to use. Bis(trifluoromethane)sulfonimide lithium (LiTFSI, 99%, Aladdin) was dried at 80 °C under vacuum before use.

### Synthesis of LC monomer (C6M)

C6M was synthesized according to previous reports.<sup>44,45</sup> Typically, 4-(6'-acryloxy-hexyloxy) benzoic acid (6.44 g, 0.022 mol) and DCC (5.96 g, 0.024 mol) were added to a round-bottom flask containing 60 mL CH<sub>2</sub>Cl<sub>2</sub>. Subsequently, the mixture of 2-methyl-hydroxy phenol (1.24 g, 10 mmol) and DMAP (0.28 g, 2 mmol) (dissolved in CH<sub>2</sub>Cl<sub>2</sub>) was dropped into the flask and stirred for two days at room temperature. After the reaction, the insoluble salts in the solution were removed by filtering. The obtained solution was further washed by HCl (5 wt% water solution) and NaHCO<sub>3</sub> (5 wt% water solution) three times, in sequence. The residue was recrystallized with isopropanol over 5 times. Finally, the product as a white solid (C6M) was obtained. <sup>1</sup>H NMR (400 MHz, CDCl<sub>3</sub>, δ, ppm): 8.11 (4H, t), 7.17–7.05 (3H, m), 6.96 (4H, q), 6.42 (1H, d), 6.38 (1H, d), 6.15–6.08 (2H, q), 5.84 (1H, d), 5.81 (1H, d), 4.17 (4H, t), 4.04 (4H, t), 2.23 (3H, s), 1.84 (4H, m), 1.72 (4H, m), 1.66–1.36 (8H, m).

### Preparation of composite solid-state polymer electrolyte film using liquid crystal and ionic liquid

The solid-state composite polymer electrolyte was prepared *via* a facile photopolymerization method. In this study, C6M was used not only as a novel active monomer but also to construct ordered ion channels. In addition, an ionic liquid was used to effectively transport ions. Typically, LC (C6M, 0.5 g) and IL (1 g) were added to a sample bottle containing THF (8 mL), LiTFSI (0.3 g) and 1-hydroxycyclohexyl phenyl ketone (4 wt% of C6M, photoinitiator). After stirring for 10 min, the solution was casted onto a polytetrafluoroethylene mould. The sample was exposed to a 365 nm UV light (GGJ-X1000, Lamp power is 1 KW) for 5 min. Finally, the flexible electrolyte films were dried at 60 °C under vacuum condition for 24 h and named as PLC-IL-1-2. Similarly, PLC-IL-1-1 was obtained. For comparison,

a PEGDA-based electrolyte film was also prepared in the same way.

### Characterization

$^1\text{H}$  NMR spectra were recorded on a JNM-ECZ400S (JEOL, 400 MHz) spectrometer at 25 °C with tetramethylsilane (TMS) as the internal standard and deuteriochloroform ( $\text{CDCl}_3$ ) as the solvent. FTIR analyses were conducted on a Thermo Nicolet AVATAR 360 infrared spectrum analyzer from 4000 to 500  $\text{cm}^{-1}$ . Thermogravimetric analysis (TGA) was obtained under  $\text{N}_2$  atmosphere on a TA600 instrument from 50 to 600 °C (heating rate of 20 °C  $\text{min}^{-1}$ ). DSC measurements were recorded from -90 to 150 °C at a heating/cooling rate of 10 °C  $\text{min}^{-1}$  under  $\text{N}_2$  atmosphere using a Q2000 instrument while an empty pan was used as a reference. The samples (4–6 mg) were sealed in aluminium pans during the tests. To determine the microstructure of the electrolyte films (the samples were sputtered with Au for 30 s), SEM (Hitachi SU8010) was employed to characterize the samples. Leica DM2700P polarizing optical microscopy (POM) with a LNP95 heating and cooling stage (the heating or cooling rate was 10 °C  $\text{min}^{-1}$ ) was used to observe the texture structures of the series samples. Specifically, the samples were sandwiched between two circular slides, whose thickness and diameter were 0.14 and 15 mm, respectively. We performed X-ray diffraction (XRD) measurements on an Automated Multipurpose X-ray Diffractometer Smartlab 9 kW operating at 45 kV and 200 mA with a copper target ( $\lambda = 1.54 \text{ \AA}$ ). Moreover, for the XRD tests, the scanning rate was 3°  $\text{min}^{-1}$  from 2° to 15°, and the as-prepared electrolyte film had a thickness of about 80  $\mu\text{m}$ .

### Electrochemical measurements

Ionic conductivities of the PLC-IL-1-1 and PLC-IL-1-2 were investigated using alternating-current (AC) impedance analysis on a symmetrical cell of stainless steel (SS)/electrolyte/SS with a frequency range from 1 Hz to 1 MHz (amplitude of 5 mV) using a Zennium Electrochemical workstation (Zahner-Ennium). The testing temperatures were in the range from 30 to 80 °C with a step size of 10 °C  $\text{min}^{-1}$ . The SS/electrolyte/SS cell was kept at every testing temperature for half-hour before tests. Then, the ionic conductivity was calculated by eqn (1):

$$\sigma = \frac{L}{SR} \quad (1)$$

where  $S$  is the contact area of electrolytes and electrode,  $L$  is the thickness of electrolyte films, and  $R$  is the bulk resistance of electrolyte films.

The linear sweep voltammogram (LSV) analysis was performed on a cell of SS/electrolyte/Li to explore the electrochemical stability of PLC-IL-1-1 and PLC-IL-1-2 at a scan rate of 5  $\text{mV s}^{-1}$  using the Zennium Electrochemical workstation.

AC impedance spectra were recorded on a symmetrical cell of Li/PLC-IL-1-2/Li at 30 °C after different storing times to evaluate the interfacial compatibility of the PLC-IL-1-2 with Li metal. The measurements were implemented in the frequency range from

0.1 Hz to 1 MHz with an oscillation voltage of 5 mV using the Zennium Electrochemical workstation.

The lithium stripping/plating experiments for Li/PLC-IL-1-2/Li symmetrical cell was conducted at 30 °C at the current density of 25  $\mu\text{A cm}^{-2}$  (the charge and discharge times were 6 h, respectively) and 50  $\mu\text{A cm}^{-2}$  (the charge and discharge times were 2 h, respectively).

In addition, the 2025 coin-type cell was assembled by Li metal anode, LFP-based cathode and the solid electrolyte (PLC-IL-1-2 or PLC-IL-1-1). The process was performed in the Ar-filled glovebox (MB-Labstar 1200/780) with  $\text{O}_2$  and  $\text{H}_2\text{O}$  contents below 0.5 ppm. The cathode was prepared by mixing LFP (70 wt% Pulead Technology Industry Co., Ltd), Super-P (20 wt%) and PVDF (10 wt%). The active substance content of the cathode was about 1.5–2  $\text{mg cm}^{-2}$ . The voltage was set in the range of 2.5 to 4.0 V on a LANHE CT2001A battery testing system for the galvanostatic charge–discharge measurements of the coin cells.

In addition, the VTF model has the following equation:

$$\sigma = A T^{-1/2} \exp\left(\frac{-E_a}{R(T - T_0)}\right) \quad (2)$$

In the equation,  $A$  is a pre-exponential factor that is connected with the number of charge carriers.  $E_a$  is the activation energy related to the critical free volume for ion transport,  $R$  is the Boltzmann constant, and  $T_0$  is a parameter, typically 50 K below the glass transition temperature.

### Conflicts of interest

There are no conflicts to declare.

### Acknowledgements

We are thankful for the help from the analysis and testing center at the University of Chinese Academy of Sciences. The authors also express thanks for the support of the National Natural Science Foundation of China (No. 51073170) and Innovation Program of CAS Combination of Molecular Science and Education.

### Notes and references

- 1 J. B. Goodenough and K.-S. Park, *J. Am. Chem. Soc.*, 2013, **135**, 1167–1176.
- 2 G. Zhou, F. Li and H.-M. Cheng, *Energy Environ. Sci.*, 2014, **7**, 1307–1338.
- 3 C. Sun, J. Liu, Y. Gong, D. P. Wilkinson and J. Zhang, *Nano Energy*, 2017, **33**, 363–386.
- 4 R. Bouchet, S. Maria, R. Meziane, A. Aboulaich, L. Lienafa, J.-P. Bonnet, T. N. Phan, D. Bertin, D. Gignès and D. Devaux, *Nat. Mater.*, 2013, **12**, 452.
- 5 N. Chen, Y. Dai, Y. Xing, L. Wang, C. Guo, R. Chen, S. Guo and F. Wu, *Energy Environ. Sci.*, 2017, **10**, 1660–1667.
- 6 S. Li, Y.-M. Chen, W. Liang, Y. Shao, K. Liu, Z. Nikolov and Y. Zhu, *Joule*, 2018, **2**, 1838–1856.

- 7 L. Yue, J. Ma, J. Zhang, J. Zhao, S. Dong, Z. Liu, G. Cui and L. Chen, *Energy Storage Mater.*, 2016, **5**, 139–164.
- 8 Z. Xue, D. He and X. Xie, *J. Mater. Chem. A*, 2015, **3**, 19218–19253.
- 9 K. Xu, *Chem. Rev.*, 2014, **114**, 11503–11618.
- 10 M. Chintapalli, X. C. Chen, J. L. Thelen, A. A. Teran, X. Wang, B. A. Garetz and N. P. Balsara, *Macromolecules*, 2014, **47**, 5424–5431.
- 11 J. Mindemark, M. J. Lacey, T. Bowden and D. Brandell, *Prog. Polym. Sci.*, 2018, **81**, 114–143.
- 12 K. Binnemans, *Chem. Rev.*, 2005, **105**, 4148–4204.
- 13 T. Kato, *Science*, 2002, **295**, 2414–2418.
- 14 C. Tschierske, *Angew. Chem., Int. Ed.*, 2013, **52**, 8828–8878.
- 15 T. Kato, N. Mizoshita and K. Kishimoto, *Angew. Chem., Int. Ed.*, 2006, **45**, 38–68.
- 16 T. Kato, M. Yoshio, T. Ichikawa, B. Soberats, H. Ohno and M. Funahashi, *Nat. Rev. Mater.*, 2017, **2**, 17001.
- 17 T. Kato, *Angew. Chem., Int. Ed.*, 2010, **49**, 7847–7848.
- 18 S. W. Kang, S. H. Jin, L. C. Chien and S. Sprunt, *Adv. Funct. Mater.*, 2004, **14**, 329–334.
- 19 K. Akagi, G. Piao, S. Kaneko, K. Sakamaki, H. Shirakawa and M. Kyotani, *Science*, 1998, **282**, 1683–1686.
- 20 L. Long, S. Wang, M. Xiao and Y. Meng, *J. Mater. Chem. A*, 2016, **4**, 10038–10069.
- 21 K. Kishimoto, T. Suzawa, T. Yokota, T. Mukai, H. Ohno and T. Kato, *J. Am. Chem. Soc.*, 2005, **127**, 15618–15623.
- 22 M. Yoshio, T. Kagata, K. Hoshino, T. Mukai, H. Ohno and T. Kato, *J. Am. Chem. Soc.*, 2006, **128**, 5570–5577.
- 23 T. Ichikawa, M. Yoshio, A. Hamasaki, J. Kagimoto, H. Ohno and T. Kato, *J. Am. Chem. Soc.*, 2011, **133**, 2163–2169.
- 24 J. Sakuda, E. Hosono, M. Yoshio, T. Ichikawa, T. Matsumoto, H. Ohno, H. Zhou and T. Kato, *Adv. Funct. Mater.*, 2015, **25**, 1206–1212.
- 25 H. Shimura, M. Yoshio, K. Hoshino, T. Mukai, H. Ohno and T. Kato, *J. Am. Chem. Soc.*, 2008, **130**, 1759–1765.
- 26 S. Wang, A. Wang, X. Liu, H. Xu, J. Chen and L. Zhang, *Electrochim. Acta*, 2018, **259**, 213–224.
- 27 S. Wang, A. Wang, C. Yang, R. Gao, X. Liu, J. Chen, Z. Wang, Q. Zeng, X. Liu and H. Zhou, *J. Power Sources*, 2018, **395**, 137–147.
- 28 S. Wang, X. Liu, A. Wang, Z. Wang, J. Chen, Q. Zeng, X. Jiang, H. Zhou and L. Zhang, *ACS Appl. Mater. Interfaces*, 2018, **10**, 25273–25284.
- 29 S. Wang, X. Liu, A. Wang, Z. Wang, J. Chen, Q. Zeng, X. Wang and L. Zhang, *Polym. Chem.*, 2018, **9**, 4674–4682.
- 30 T. J. White and D. J. Broer, *Nat. Mater.*, 2015, **14**, 1087–1098.
- 31 Q. Yang, Z. Zhang, X.-G. Sun, Y.-S. Hu, H. Xing and S. Dai, *Chem. Soc. Rev.*, 2018, **47**, 2020–2064.
- 32 X. Lin, M. Salari, L. M. R. Arava, P. M. Ajayan and M. W. Grinstaff, *Chem. Soc. Rev.*, 2016, **45**, 5848–5887.
- 33 D. Zhou, R. Liu, J. Zhang, X. Qi, Y.-B. He, B. Li, Q.-H. Yang, Y.-S. Hu and F. Kang, *Nano Energy*, 2017, **33**, 45–54.
- 34 S. Wang, Q. X. Shi, Y. S. Ye, Y. Xue, Y. Wang, H. Y. Peng, X. L. Xie and Y. W. Mai, *Nano Energy*, 2017, **33**, 110–123.
- 35 J. L. Pablos, N. Garcia, L. Garrido, J. Guzman, F. Catalina, T. Corrales and P. Tiemblo, *J. Membr. Sci.*, 2018, **545**, 133–139.
- 36 J. Zhang, C. Ma, Q. Xia, J. Liu, Z. Ding, M. Xu, L. Chen and W. Wei, *J. Membr. Sci.*, 2016, **497**, 259–269.
- 37 O. Garcia-Calvo, N. Lago, S. Devaraj and M. Armand, *Electrochim. Acta*, 2016, **220**, 587–594.
- 38 J. Hu, W. Wang, H. Peng, M. Guo, Y. Feng, Z. Xue, Y. Ye and X. Xie, *Macromolecules*, 2017, **50**, 1970–1980.
- 39 Z. Wang, S. Wang, A. Wang, X. Liu, J. Chen, Q. Zeng, L. Zhang, W. Liu and L. Zhang, *J. Mater. Chem. A*, 2018, **6**, 17227–17234.
- 40 K. Yin, Z. Zhang, X. Li, L. Yang, K. Tachibana and S.-i. Hirano, *J. Mater. Chem. A*, 2015, **3**, 170–178.
- 41 M. Yasuniwa, S. Tsubakihara, Y. Sugimoto and C. Nakafuku, *J. Polym. Sci., Part B: Polym. Phys.*, 2004, **42**, 25–32.
- 42 W. Feng, D. J. Broer and D. Liu, *Adv. Mater.*, 2018, **30**, 1704970.
- 43 D.-G. Kang, D.-Y. Kim, M. Park, Y.-J. Choi, P. Im, J.-H. Lee, S.-W. Kang and K.-U. Jeong, *Macromolecules*, 2015, **48**, 898–907.
- 44 D. M. Smith, Q. Pan, S. Cheng, W. Wang, T. J. Bunning and C. Y. Li, *Adv. Mater. Interfaces*, 2018, **5**, 1700861.
- 45 X. Chen, L. Wang, Y. Chen, C. Li, G. Hou, X. Liu, X. Zhang, W. He and H. Yang, *Chem. Commun.*, 2014, **50**, 691–694.